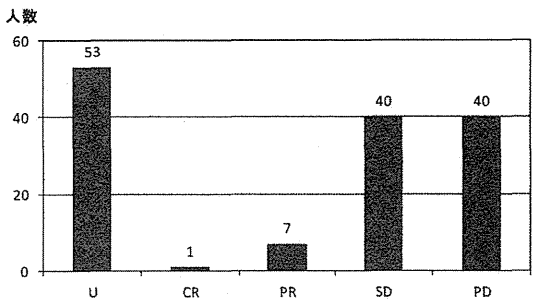

図16. 結腸・直腸がん

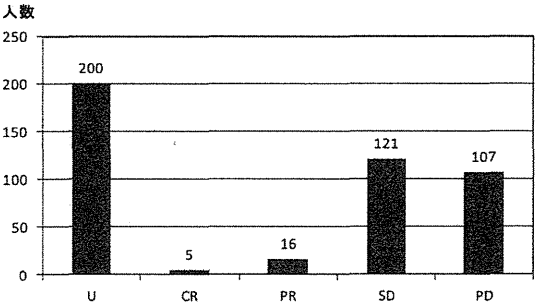

図17. 卵巣がん

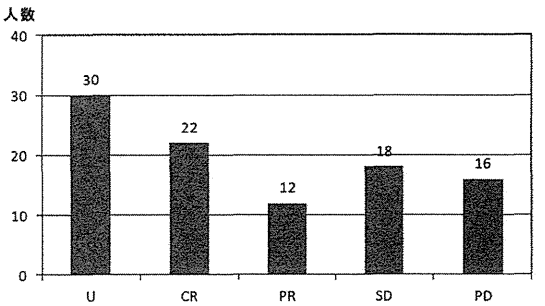

図18. 子宮頸がん

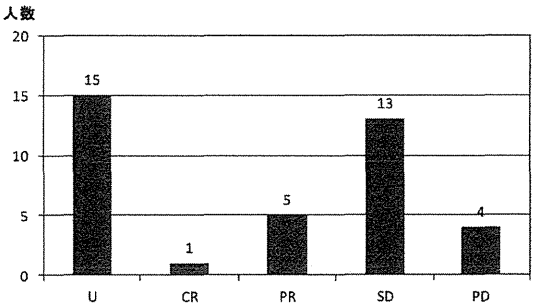

図19. 軟部組織腫瘍

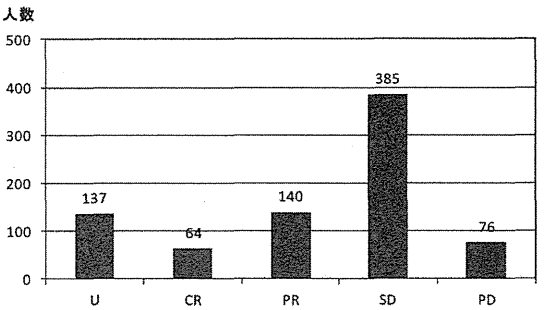

図20. 転移性がん

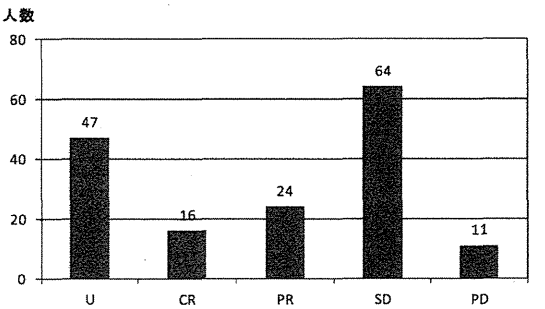

図21. 再発がん

対象疾患別の治療評価は評価不能を除いて食道がん，子宮頸がんで奏効率 (CR＋PR) が高かった．いずれの疾患も不変 (SD) が多いが，悪性腫瘍を対象として腫瘍の増大・進展が抑えられている点は特筆に値すると思われる．

2－5．治療方法

治療方法の分類は①温熱療法単独，②温熱＋放射線療法，③温熱＋化学療法，④温熱＋免疫療法，⑤温熱＋免疫＋化学療法，⑥温熱＋放射線＋免疫＋化学療法，⑦温熱＋放射線＋化学療法，⑧温熱＋放射線＋免疫療法，⑨その他，とした．

表 3．温熱単独療法と併用療法

治療方法	年 (年度)				
	2007	2008	2009	2010	2011
①温熱療法単独	508	661	816	885	989
②温熱＋放射線療法	74	66	54	73	71
③温熱＋化学療法	353	448	519	688	798
④温熱＋免疫療法	94	194	202	263	285
⑤温熱＋免疫＋化学療法	107	218	259	299	284
⑥温熱＋放射線＋免疫＋化学療法	36	74	84	62	67
⑦温熱＋放射線＋化学療法	74	140	104	144	123
⑧温熱＋放射線＋免疫療法	0	1	0	3	2
⑨その他	44	51	54	66	75

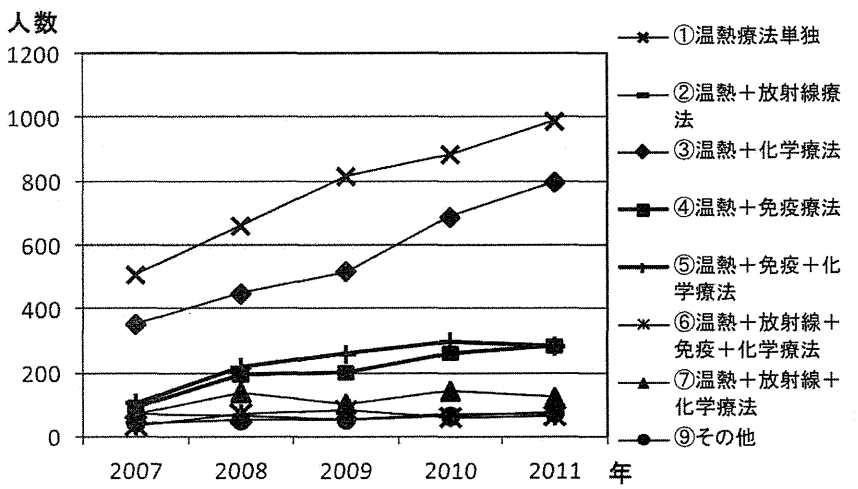

図22. 温熱単独療法と併用療法の推移

2－6．加温回数

① 最少加温回数は施設により 1 回/人から 8 回/人となっていた．そのうち 1 回/人は 80%を占めていた．

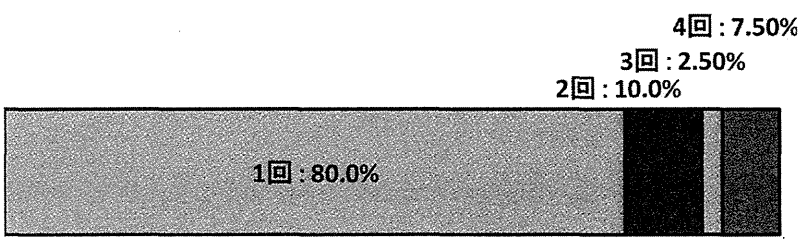

図23. 最少加温回数 (加温回数/人)

② 最多加温回数は施設により 3 回/人から 388 回/人となっていた. そのうち 100 回/人以内で 62.5%を占めていた.

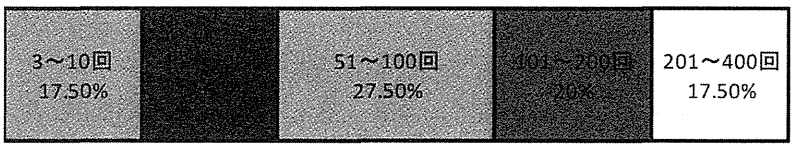

図24. 最多加温回数 (加温回数/人)

2-7. 加温期間

① 最短加温期間は施設により 1ヶ月未満から 2ヶ月となっていた. 最も多かったのは 1ヶ月の 51.3%であった.

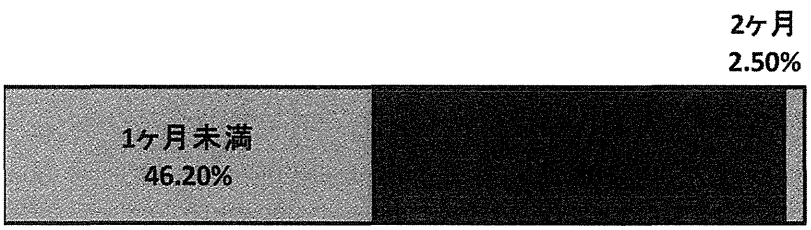

図25. 最短加温治療期間 (月)

② 最長加温期間は施設により 1.5ヶ月から 106ヶ月となっていた. 最も多かったのは 1～10ヶ月の 32.5%であった.

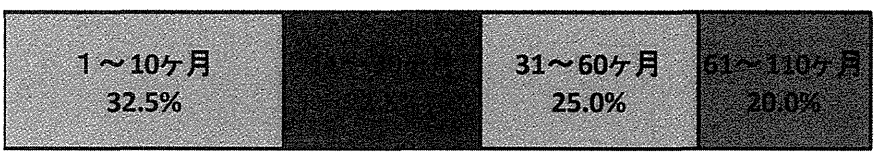

図26. 最長加温治療期間 (月)

2-8. 保険申請方法と採択率

回答少なく統計処理できなかった.

2-9. スタッフ数

回答には施設全体のスタッフ数と温熱治療を担当するスタッフ数が混在しており統計処理できなかった.

2-10. 中止された施設

回答を統計処理できなかった.

ま と め

2007～2011 年の 5 年間で，新たな実施施設と患者数の増加が認められた．治療患者総数は 5 年間で 3,195 から 12,077 と 3.8 倍に増加していた．対象疾患は脳を除く全身の臓器と多岐にわたっていた．転移性がんが最も多く，設問の関係で明らかに分けて回答されてはいないが，他の疾患にも転移性がん，進行がん，再発がんが多く含まれていると考えられた．治療方法は温熱療法単独が最も多く，次いで化学療法との併用，免疫療法との併用，放射線との併用であった．温熱療法単独例の中には温熱療法と化学療法が別々の施設にて行われている症例も含まれると考えられ，化学療法との併用例は実際には報告数よりも多いと考えられた．温熱療法の平均回数は 10 回前後であった．最大加温回数は，51～100 回，27.50%，101～200 回 20%，201～400 回 17.50%であった．50 回以上の加温は 1 年以上にわたって加温された症例と考えられ，長期間治療されている症例も多いことが推察された．治療の評価は 5 段階評価が報告された施設のデータのみを使用した．SD 例が多く CR と PR は少なかった．奏功例 (CR＋PR) の多くは子宮頸がん，食道がんにて認められた．放射線治療が可能な大病院を除く一般病院やクリニックでは，根治的な治療は困難な進行例や再発例が多いことを考慮すれば，SD 例が多いことは QOL の改善と生存期間の延長に寄与している可能性もあり，温熱療法の意義があると考えられた．

^{62}Cu-Diacetyl-Bis (N^4-Methylthiosemicarbazone) PET in Human Gliomas: Comparative Study with [^{18}F]Fluorodeoxyglucose and L-Methyl-[^{11}C]Methionine PET

K. Tateishi, U. Tateishi, S. Nakanowatari, M. Ohtake, R. Minamimoto, J. Suenaga, H. Murata, K. Kubota, T. Inoue, and N. Kawahara

ABSTRACT

BACKGROUND AND PURPOSE: ^{62}Cu-diacetyl-bis(N^4-methylthiosemicarbazone) was developed as a hypoxic radiotracer in PET. We compared imaging features among MR imaging and ^{62}Cu-diacetyl-bis(N^4-methylthiosemicarbazone)-PET, FDG-PET, and L-methyl-[^{11}C]methionine)-PET in gliomas.

MATERIALS AND METHODS: We enrolled 23 patients who underwent ^{62}Cu-diacetyl-bis(N^4-methylthiosemicarbazone)-PET and FDG-PET and 19 (82.6%) who underwent L-methyl-[^{11}C]methionine)–PET, with all 23 patients undergoing surgery and their diagnosis being then confirmed by histologic examination as a glioma. Semiquantitative and volumetric analysis were used for the comparison.

RESULTS: There were 10 newly diagnosed glioblastoma multiforme and 13 nonglioblastoma multiforme (grades II and III), including 4 recurrences without any adjuvant treatment. The maximum standardized uptake value and tumor/background ratios of ^{62}Cu-diacetyl-bis(N^4-methylthiosemicarbazone), as well as L-methyl-[^{11}C]methionine, were significantly higher in glioblastoma multiforme than in non-glioblastoma multiforme ($P = .03$ and $P = .03$, respectively); no significant differences were observed on FDG. At a tumor/background ratio cutoff threshold of 1.9, ^{62}Cu-diacetyl-bis(N^4-methylthiosemicarbazone) was most predictive of glioblastoma multiforme, with 90.0% sensitivity and 76.9% specificity. The positive and negative predictive values, respectively, for glioblastoma multiforme were 75.0% and 85.7% on ^{62}Cu-diacetyl-bis(N^4-methylthiosemicarbazone), 83.3% and 60.0% on L-methyl-[^{11}C]methionine, and 72.7% and 75.0% on MR imaging. In glioblastoma multiforme, volumetric analysis demonstrated that ^{62}Cu-diacetyl-bis(N^4-methylthiosemicarbazone) uptake had significant correlations with FDG ($r = 0.68$, $P = .03$) and L-methyl-[^{11}C]methionine ($r = 0.87$, $P = .03$). However, the ^{62}Cu-diacetyl-bis(N^4-methylthiosemicarbazone)–active region was heterogeneously distributed in 50.0% (5/10) of FDG-active and 0% (0/6) of L-methyl-[^{11}C]methionine)–active regions.

CONCLUSIONS: ^{62}Cu-diacetyl-bis(N^4-methylthiosemicarbazone) may be a practical radiotracer in the prediction of glioblastoma multiforme. In addition to FDG-PET, L-methyl-[^{11}C]methionine)–PET, and MR imaging, ^{62}Cu-diacetyl-bis(N^4-methylthiosemicarbazone)-PET may provide intratumoral hypoxic information useful in establishing targeted therapeutic strategies for patients with glioblastoma multiforme.

ABBREVIATIONS: ^{62}Cu-ATSM = ^{62}Cu-diacetyl-bis(N^4-methylthiosemicarbazone); GBM = glioblastoma multiforme; MET = L-methyl-[^{11}C]methionine; non-GBM gliomas = World Health Organization grade II and III gliomas; SUV_{max} = maximum standardized uptake value; T/B ratio = tumor/background ratio

Gliomas have heterogeneously infiltrative and proliferative features, among which glioblastoma multiforme (GBM) is the most common and has the worst prognosis in adults.[1] From a histopathologic standpoint, microvascular proliferation and/or necrosis is essential for the diagnosis of GBM.[1] However, random tissue sampling may not always lead to an accurate diagnosis because of tissue heterogeneity. Therefore, other diagnostic modalities to predict highly malignant regions, such as PET imaging, can provide complementary diagnostic and therapeutic information and guide selective target tissue sampling or resection.

Malignant tumor cells display an increased flux of glucose metabolism by increased expression of glucose transporters and hexokinase, as well as an increased rate of amino acid uptake and metabolism.[2] This increased transport and high metabolism oc-

Received April 3, 2013; accepted after revision June 2.

From the Departments of Neurosurgery (K.T., S.N., M.O., J.S., H.M., N.K.) and Radiology (U.T., T.I.), Graduate School of Medicine, Yokohama City University, Yokohama, Japan; and Division of Nuclear Medicine (R.M., K.K.), Department of Radiology, National Center for Global Health and Medicine, Tokyo, Japan.

This work was supported by Japan Advanced Molecular Imaging Program (J-AMP) of the Ministry of Education, Culture, Sports, Science and Technology (MEXT), Japan, and was partly funded by a Grant-in-Aid for Scientific Research from the Japan Society for the Promotion of Sciences (No. 24791515).

Please send correspondence to Nobutaka Kawahara, MD, PhD, Department of Neurosurgery, Graduate School of Medicine, Yokohama City University, 3–9 Fukuura, Kanazawa-ku, Yokohama, Kanagawa 236-0004, Japan; e-mail: nkawa@yokohama-cu.ac.jp

Indicates open access to non-subscribers at www.ajnr.org
Indicates article with supplemental on-line tables.
Indicates article with supplemental on-line figure.
http://dx.doi.org/10.3174/ajnr.A3679

cur commonly in GBM and can be detected by widely used techniques, such as FDG-PET and L-methyl-[^{11}C]methionine (MET)-PET.[3-9] However, the predictive value of these PET imaging techniques has not been adequate for a diagnosis of GBM because uptake of these tracers is not specific in GBM.[3,4] On the other hand, tissue hypoxia and necrosis are cardinal features of GBM that are often associated with resistance to radiation therapy and chemotherapy.[10] Thus, intratumoral hypoxic information may be useful for an accurate diagnosis and establishment of effective therapeutic strategies for gliomas.

Some clinical investigations by use of [^{18}F]fluoromisonidazole-PET have been recently undertaken to detect tissue hypoxia noninvasively in gliomas.[11-13] On the other hand, we previously reported the clinical usefulness of ^{62}Cu-diacetyl-bis(N^4-methylthiosemicarbazone) (^{62}Cu-ATSM)-PET imaging for gliomas.[14] Our preliminary study revealed a relationship between ^{62}Cu-ATSM uptake values and hypoxia-inducible factor-1α expression, which is increased under hypoxia,[14] suggesting that ^{62}Cu-ATSM-PET is a practical hypoxic imaging technique in gliomas. However, whether ^{62}Cu-ATSM uptake is specific in GBM was not determined, and the correlation of ^{62}Cu-ATSM findings with FDG and MET remained unclear in GBM. In addition, to assess whether ^{62}Cu-ATSM uptake is dependent on BBB breakdown and to evaluate an additional value over MR imaging findings, we volumetrically and qualitatively compared ^{62}Cu-ATSM-PET imaging with T1-weighted MR imaging with Gd-DTPA.

MATERIALS AND METHODS

Patients

This study was approved by the local ethics committee (Institutional Review Board no. B1001111026) after written informed consent was obtained from all patients. Between December 2010 and December 2012, we prospectively performed ^{62}Cu-ATSM-PET in 68 patients with malignant brain tumors. Among them, 23 consecutive patients with pathologically confirmed gliomas (10 men and 13 women; age range, 19–81 years; mean age, 54.2 ± 17.5 years) who received FDG-PET and/or MET-PET with ^{62}Cu-ATSM-PET were retrospectively analyzed. FDG-PET and MET-PET imaging were performed in 23 patients (100%) and 19 patients (82.6%), respectively. Of the 23 patients, 19 (82.6%) were newly diagnosed, and the remaining 4 patients (17.4%), who previously underwent biopsy but had not received any radiation therapy or chemotherapy, were diagnosed as having tumor recurrence. Histologic diagnosis and tumor grade were classified according to the following 2007 World Health Organization criteria: 8 (34.8%) grade II (3 diffuse astrocytomas, 3 oligoastrocytomas, and 2 oligodendrogliomas); 5 (21.7%) grade III (1 anaplastic oligoastrocytoma and 4 anaplastic oligodendrogliomas); and 10 (43.5%) grade IV (GBM). All 10 patients with GBM were newly diagnosed. Thirteen grade II and III gliomas (56.5%) were classified as non-GBM gliomas. The oligodendroglial component was found in 10 (76.9%) of 13 non-GBM gliomas.

Intervals from the MR imaging investigation to ^{62}Cu-ATSM-PET, FDG-PET, and MET-PET were 5.4 ± 4.1, 4.3 ± 3.2, and 5.4 ± 3.4 days, respectively (mean ± SD). All patients underwent surgery the day after a repeated MR imaging study for neuronavigation, and their diagnosis was confirmed on histologic examination. On-Line Table 1 summarizes the patient characteristics.

PET and MR Image Acquisition

Preparation of ^{62}Cu-ATSM, FDG, and MET has been described in previous reports.[15,16] To acquire ^{62}Cu-ATSM-PET and FDG-PET/CT images, a whole-body PET/CT scanner (Aquiduo PCA-7000B; Toshiba, Tokyo, Japan) with a 16-row detector in the CT component was used at the Yokohama City University Hospital (Yokohama, Japan). MET-PET imaging was performed with PET/CT scans (Biograph 16; Siemens, Erlangen, Germany) at the National Center for Global Health and Medicine (Tokyo, Japan). An image quality phantom (NU 2–2001; National Electrical Manufacturers Association) was used for cross-calibration because such phantoms are widely used and allow estimation of optimal acquisition times.

For ^{62}Cu-ATSM-PET/CT and FDG-PET/CT, the following conditions were used for acquisition of low-dose CT data: 120 kVp, an auto-exposure control system, a beam pitch of 0.875 or 1, and a 1.5- or 2-mm × 16-row mode. No iodinated contrast material was administered. After intravenous injection of 740 MBq of ^{62}Cu-ATSM, the patients were placed in a supine "arm-up" position. Dynamic data acquisition was carried out for 30–40 minutes, and PET/CT images were reconstructed from the data. For studies of FDG, the patients received an intravenous injection of 370 MBq of FDG after at least 6 hours of fasting, followed by an uptake phase of approximately 60 minutes. For MET-PET/CT, the following conditions were used for acquisition of low-dose CT data: 120 kVp, an auto-exposure control system, a beam pitch of 0.875, and a 3-mm × 16-row mode. After 6 hours of fasting, 370 MBq of MET was intravenously injected, followed by data acquisition at 20 minutes after the injection. The following acquisition settings were used for ^{62}Cu-ATSM-PET/CT and FDG-PET/CT: 3D data acquisition mode; 180 seconds/bed; field of view, 500 mm; 4 iterations; 14 subsets; matrix size, 128 × 128; 8-mm Gaussian filter, full width at half maximum; and reconstruction, ordered subset expectation maximization. For MET-PET/CT, the following acquisition settings were used: 3D data acquisition mode; 180 seconds/bed; field of view, 300 mm; 4 iterations; 14 subsets; matrix size, 256 × 256; 4-mm Gaussian filter, full width at half maximum; and reconstruction, ordered subset expectation maximization. The estimated internal absorbed doses of ^{62}Cu-ATSM, FDG, and MET were approximately 10, 2.5, and 1.9 mSv, respectively.

MR imaging was performed on a 1.5T system (Magnetom Symphony; Siemens). 3D T1-weighted MR imaging with a MPRAGE sequence was used with the following parameters to acquire axial T1-weighted images after administration of 0.2 mL/kg of Gd-DTPA: field of view, 250 × 250 mm^2; matrix size, 512 × 512; TR, 1960 ms; TE, 3.9 ms; TI, 1100 ms; and flip angle, 15°. In total, 120 contiguous 2-mm images were obtained from each patient.

Image Interpretation

Four board-certified nuclear medicine specialists who were unaware of the clinical information assessed the PET images semiquantitatively and volumetrically in consensus (^{62}Cu-ATSM and

FDG, U.T. and T.I.; MET, R.M. and T.I.). MR imaging findings were also assessed by board-certified radiologists (U.T. and T.I.), who interpreted the tumors as either GBM or non-GBM gliomas. A volume of interest was outlined within areas of increased tracer uptake and was measured on each section. In extensively heterogeneous lesions, regions of interest covered all components. For semiquantitative interpretations, the standardized uptake value was determined by a standard formula. The tumor/background ratio (T/B ratio) of ^{62}Cu-ATSM and MET was calculated relative to the uptake in the contralateral frontal cortex. The FDG T/B ratio was calculated relative to the uptake in the contralateral white matter. The uptake values of the ^{62}Cu-ATSM, FDG, and MET tracers were determined by assessment of the maximum standardized uptake value (SUV_{max}) values and T/B ratios.

Dr. View version R 2.5 for LINUX (Infocom, Tokyo, Japan) software was used to merge the PET images with the MR images,[4,13,14] and each PET and MR image was volumetrically compared. To evaluate volumetric analysis, we extracted the uptake regions of the ^{62}Cu-ATSM images on the basis of the optimal T/B ratio thresholds of ≥1.8, a cutoff value for predicting hypoxia-inducible factor-1α expression in our previous study.[14] The uptake regions of the FDG and MET images were extracted on the basis of the T/B ratio thresholds of ≥1.5 and ≥1.3, respectively, in accordance with previous reports.[5,9] These uptake regions were rated as metabolically active volumes. For GBM, we extracted the tumor volume by measuring a completely covered contrast-enhanced region with necrotic and cystic components on MR imaging. The contrast-enhanced volume was also separately extracted by measuring a contrast-enhanced region without any necrotic and cystic components. Metabolically active regions shown by each PET tracer were overlaid on the MR images for qualitatively comparing metabolically active regions among the 3 tracers. Tumors with ^{62}Cu-ATSM–active regions that demonstrated ≤50% volumetric overlap with the active regions of FDG and MET were rated as heterogeneous with respect to intratumoral oxygenation. Correlations among ^{62}Cu-ATSM, FDG, and MET were also volumetrically analyzed. On the basis of the optimal cutoff value for prediction of GBM (T/B ratio, 1.9), which was defined by receiver operating characteristic analysis, tumors having ^{62}Cu-ATSM T/B ratios ≥1.9 were rated as GBM. The optimal cutoff threshold of the MET T/B ratio was set by receiver operating characteristic analysis, and tumors having MET T/B ratios ≥3.0 were rated as GBM. To assess the clinical value of ^{62}Cu-ATSM-PET findings relative to those of MET-PET and MR imaging findings for prediction of GBMs, we evaluated the positive and negative predictive values independently.

Statistical Analysis

All parameters were expressed as means ± SDs. Two-way repeated measures ANOVA was used to compare the mean uptake values of each tracer. To determine the optimal radiotracer for prediction of GBM by semiquantitative analysis, we performed receiver operating characteristic analysis. To evaluate volumetric correlations of ^{62}Cu-ATSM with FDG and MET, we used linear regression analysis. The Wilcoxon signed rank test was used to compare the mean tumor volume, contrast-enhanced volume, and metabolically active volumes determined by the 3 PET tracers. The Fisher exact probability test was used to compare the ^{62}Cu-ATSM-PET with contrast-enhanced MR imaging and MET-PET imaging features. The level of statistical significance was set at $P < .05$. JMP 10 statistical software (SAS Institute, Cary, North Carolina) was used for statistical analyses.

RESULTS

Semiquantitative Analysis of PET Studies According to Tumor Classification

A summary of the uptake values for each PET tracer is presented in On-Line Table 2. Representative images are shown in Fig 1 and in the On-Line Figure. The average ^{62}Cu-ATSM SUV_{max} values in GBM and non-GBM gliomas were 1.68 ± 0.94 and 0.98 ± 0.52, respectively. The ^{62}Cu-ATSM SUV_{max} was significantly higher for GBM than for non-GBM gliomas ($P = .03$; Fig 2*A*). A significant difference in SUV_{max} was also detected between GBM and non-GBM gliomas for MET (5.23 ± 1.11 and 3.25 ± 1.66, respectively; $P = .02$; Fig 2*A*) but not for FDG (7.31 ± 3.22 and 5.72 ± 2.25, respectively; $P = .18$; Fig 2*A*).

The mean ^{62}Cu-ATSM T/B ratios in GBM and non-GBM gliomas were 3.10 ± 2.37 and 1.47 ± 0.57, respectively, which were also significantly different ($P = .03$; Fig 2*B*). Receiver operating characteristic analysis indicated that a ^{62}Cu-ATSM T/B ratio cutoff threshold of 1.9 was most predictive of GBM, with 90.0% sensitivity and 76.9% specificity (area under the curve, 0.88). Similar to the SUV_{max} results, there was a significant difference in the T/B ratio between GBM and non-GBM gliomas for MET (3.53 ± 0.70 and 2.27 ± 0.97, respectively; $P = .01$; Fig 2*B*) but not for FDG (2.71 ± 1.56 and 2.44 ± 1.28, respectively; $P = .65$; Fig 2*B*). Receiver operating characteristic analysis showed an optimal T/B ratio of 3.0 for MET (sensitivity, 83.3%; specificity, 76.9%; area under the curve, 0. 83, respectively), which was slightly less than that for ^{62}Cu-ATSM.

Volumetric and Qualitative Comparison among 3 Tracers in GBM

A summary of tumor volume and contrast-enhanced volume on MR imaging and the active volume for each PET tracer is presented in On-Line Table 3. Table 1 shows the relationships of the metabolically active volumes in GBM: for ^{62}Cu-ATSM (T/B ratio ≥1.8), FDG (T/B ratio ≥1.5), and MET (T/B ratio ≥1.3); the volumes were 8.2 ± 14.0, 11.0 ± 12.0, and 38.0 ± 19.0 cm^3, respectively. The mean active volume of ^{62}Cu-ATSM in GBM was not significantly different from that of FDG ($P = .63$) but was significantly less than that of MET ($P = .03$). In addition, the active volume of ^{62}Cu-ATSM in GBM correlated significantly with that of FDG ($r = 0.68$, $P = .03$) and MET ($r = 0.87$, $P = .03$). However, compared with the active regions of FDG and MET, those of ^{62}Cu-ATSM were heterogeneously distributed (≤50% volumetric overlap with the active regions of FDG and MET) in 50% (5/10) and 0% (0/6) of the tumors with metabolically active regions, respectively. The ^{62}Cu-ATSM–active regions were fully covered within the MET-active regions in all cases.

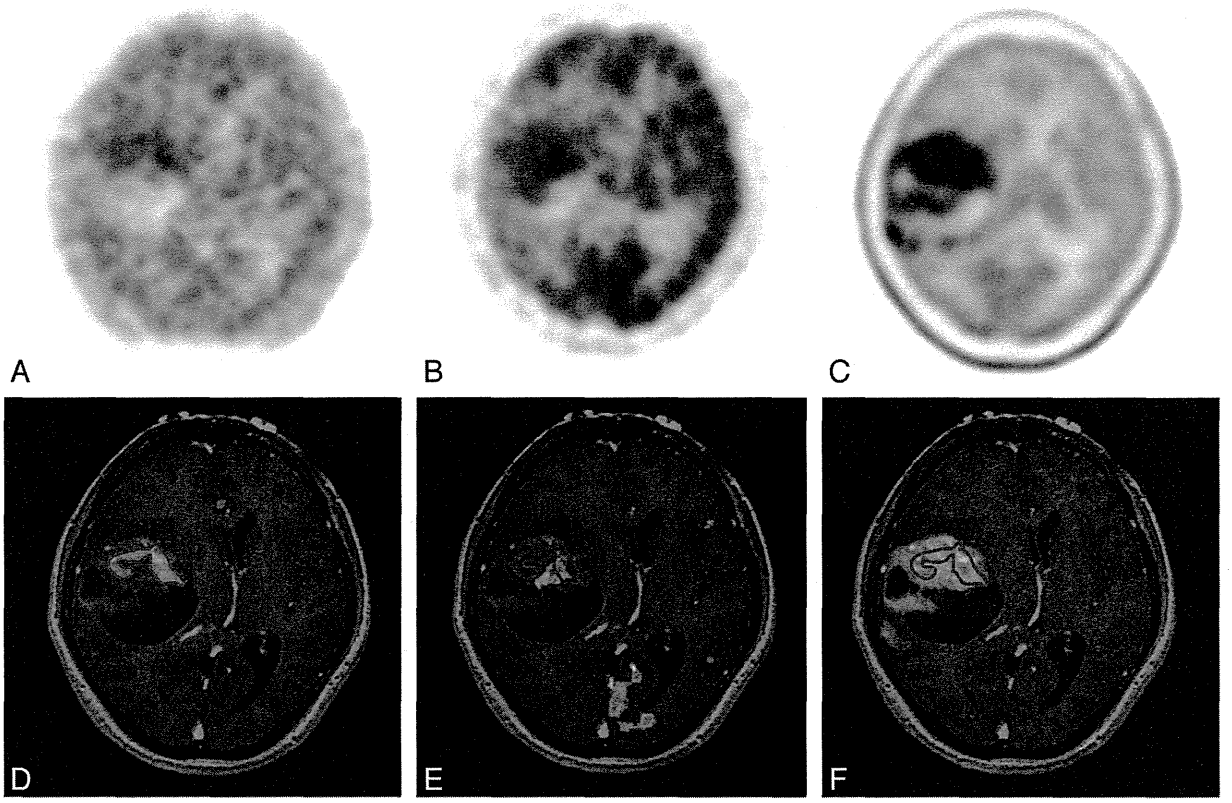

FIG 1. Case 21. A 59-year-old woman with GBM in the right temporal lobe (tumor volume, 79.6 cm^3). PET images of ^{62}Cu-ATSM (*A*), FDG (*B*), and MET (*C*) are shown; the ^{62}Cu-ATSM–active regions are outlined by red lines (*D–F*, respectively). ^{62}Cu-ATSM-PET/MR imaging fusion image (*D*) showing the intratumoral hypoxic region (11.8 cm^3), which is less than that of the contrast-enhanced volume (30.9 cm^3). FDG-PET/MR imaging fusion image (*E*) also indicating the intratumoral active region (4.6 cm^3), which is heterogeneously distributed compared with the ^{62}Cu-ATSM–active region. MET-PET/MR imaging fusion image (*F*) showing the more extensive active region (73.1 cm^3), which completely covered the ^{62}Cu-ATSM–active regions.

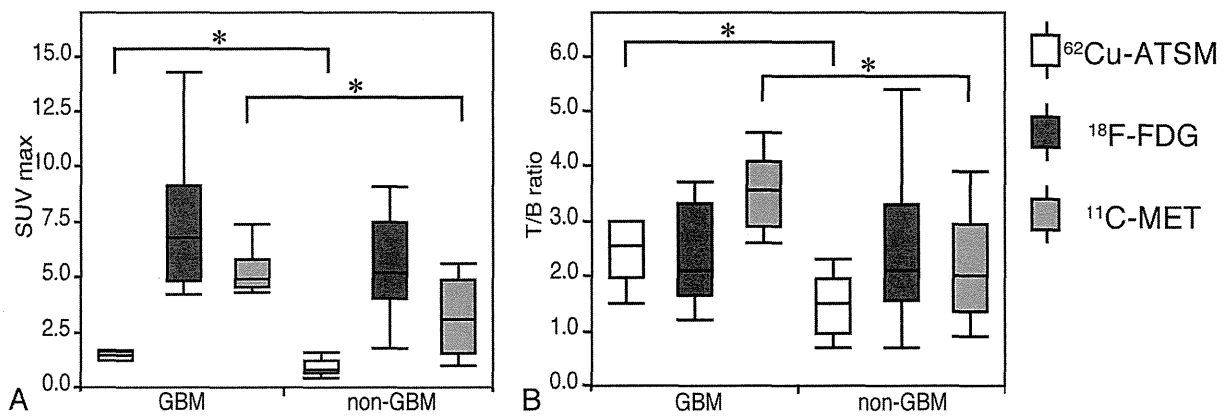

FIG 2. Boxplots comparing uptake values between GBM and non-GBM gliomas. The ^{62}Cu-ATSM and MET SUV_{max} values show significant differences ($P = .03$ and $P = .02$); however, FDG SUV_{max} values are not significantly different ($P = .18$; *A*). The ^{62}Cu-ATSM and MET T/B ratios also show significant differences ($P = .03$ and $P = .01$), but no significant difference is observed in the FDG T/B ratio ($P = .65$; *B*). *$P < .05$.

Volumetric Comparison with MR Imaging

The mean tumor volume and contrast-enhanced volume in GBMs were 45.4 ± 26.5 and 21.6 ± 14.3 cm^3, respectively (Table 2), which were significantly greater than those of the metabolically active volumes for ^{62}Cu-ATSM ($P = .002$ and $P = .002$, respectively) and FDG ($P = .002$ and $P = .006$, respectively). The mean active volume of MET was not significantly different from the mean tumor volume ($P = .56$) and contrast-enhanced volume ($P = .06$).

Predictive Values of ^{62}Cu-ATSM-PET, MET-PET, and MR Imaging for Distinguishing GBM

In 19 newly diagnosed gliomas, tumors having ^{62}Cu-ATSM–active regions and strongly contrast-enhanced regions on MR imaging

Table 1: Volumetric correlation of ^{62}Cu-ATSM with FDG and MET in GBM

GBM (n=10)	Volume (cm^3)	r	P Value	Heterogeneous Metabolism (%)[a]
^{62}Cu-ATSM	8.2 ± 14.0	—	—	—
FDG	11.0 ± 12.0	0.68	.03	5/10 (50%)
MET	38.0 ± 19.0	0.87	.03	0/6 (0%)

Note:—r indicates correlation coefficient when compared with ^{62}Cu-ATSM.
[a] Heterogeneous metabolism indicates an overlap of ≤50% of the active volume of ^{62}Cu-ATSM with those of FDG and MET.

Table 2: Volumetric comparison of radiotracers in MRI for GBM

GBM (n=10)	TV (45.4 ± 26.5 cm^3)[a]	CEV (21.6 ± 14.3 cm^3)[b]
^{62}Cu-ATSM (8.2 ± 14.0 cm^3)	P = .002	P = .002
FDG (11.0 ± 12.0 cm^3)	P = .002	P = .006
MET (38.0 ± 19.0 cm^3)	P = .56	P = .06

Note:—The mean tumor volume (TV) and contrast-enhanced volume (CEV) were compared with the active volume of ^{62}Cu-ATSM (T/B cutoff threshold ≥1.8), FDG (T/B cutoff threshold of ≥1.5), and MET (T/B cutoff threshold of ≥1.3). P values < .05 were considered to indicate statistical significance.
[a] TV was measured as a completely covered contrast-enhanced region with necrotic and cystic components.
[b] CEV was measured as a contrast-enhanced region without necrotic and cystic components on T1-weighted MRI with Gd-DTPA.

were detected in 63.2% (12/19) and 57.9% (11/19), respectively. No statistical correlation was observed between the 2 modalities (P = .07). The positive predictive values of ^{62}Cu-ATSM and MR imaging for distinguishing GBM were 75.0% and 72.7%, respectively. In contrast, the negative predictive values of ^{62}Cu-ATSM and MR imaging were 85.7% and 75.0%, respectively. On the other hand, when tested by the optimal cutoff threshold on MET (T/B ratio, 3.0), the positive and negative predictive values for a diagnosis of GBM were 83.3% and 60.0%, respectively. We found no significant correlation between ^{62}Cu-ATSM and MET (P = .59).

DISCUSSION

Our present PET study demonstrated that ^{62}Cu-ATSM is a predictive radiotracer for GBM. Many clinical PET studies with FDG and MET have been conducted to discriminate among World Health Organization grades of gliomas.[4,5,7,8] Several imaging studies have demonstrated the usefulness of FDG-PET in the differentiation between low-grade and high-grade gliomas and even between grade III and grade IV gliomas.[5,7,8] Because of the associated increased glucose uptake and high rates of glycolysis, FDG-PET shows high FDG uptake in GBM.[8] However, FDG-PET has a low signal-to-noise ratio in brain tumors, which is a result of the high glucose metabolism in normal brain tissue.[4] Moreover, because FDG uptake reflects an increased glycolytic rate in rapidly growing brain tumor cells even in grade II and III gliomas,[7,12] it may not be a suitable radiotracer to predict GBM. On the other hand, malignant gliomas demonstrate increased rates of amino acid uptake and metabolism. MET readily crosses the intact BBB through a neutral amino acid transporter and is incorporated into active tumor areas, which allows tumor visualization even in low-grade gliomas.[9]

In our current study, MET-PET revealed a significant difference between GBM and non-GBM despite the high frequency of oligodendroglial tumors. However, these oligodendroglial tumors are reported to show relatively high uptake of MET irrespective of their grade on MET-PET,[3,4] which is not yet established as a standard imaging technique for a diagnosis of GBM. Recently, another technique, hypoxic imaging, has been used clinically and may be another diagnostic tool to discriminate GBM from non-GBM gliomas because poor microcirculation with respect to metabolic demand induces relative tissue hypoxia and necrosis, a cardinal feature of GBM.[10]

Hypoxic PET studies with [^{18}F]fluoromisonidazole and ^{62}Cu-ATSM have demonstrated their usefulness separately in hypoxic imaging. Under hypoxic conditions, ^{62}Cu-ATSM retention is induced by microsomal cytochrome reductase enzymes, which is different from [^{18}F]fluoromisonidazole retention by mitochondrial nitroreductase enzymes.[17] Cu-ATSM was developed as a radiotracer to detect regional hypoxia in the ischemic myocardium and hypoxic tissues in tumors,[18,19] and its image contrast may be greater than that of [^{18}F]fluoromisonidazole, because Cu-ATSM has rapid blood clearance and is retained in hypoxic tissues with a high hypoxic/normoxic tissue-to-activity ratio.[20] On the other hand, [^{18}F]fluoromisonidazole can detect a wider range of partial oxygen tension values than ^{61}Cu-ATSM.[17] Experimental investigations with glioma models have demonstrated that ^{61,64,67}Cu-ATSM uptake correlates with tissue hypoxia.[19] Our preliminary clinical study also showed that ^{62}Cu-ATSM uptake values correlated highly with hypoxia-inducible factor-1α expression, which is a biomarker of tissue hypoxia,[14] and the optimal cutoff threshold to predict hypoxia-inducible factor-1α expression (T/B ratio, 1.8) was similar to that of our present study in the prediction of GBM (T/B ratio, 1.9). It has been well established that overexpression of hypoxia-inducible factor-1α, a transcription factor that is part of the stress response mechanism, is initiated in the presence of low oxygen tensions and induces hypoxia-regulated molecules, such as vascular endothelial growth factor, glucose transporters, and carbonic anhydrase IX,[21] which correlate with treatment resistance and are highly expressed in GBM.[10] Therefore, ^{62}Cu-ATSM-PET may be a radiotracer useful in the identification of treatment-resistant hypoxic regions in patients with glioma. Our present study also demonstrated that hypoxic imaging by use of ^{62}Cu-ATSM for discrimination of GBM from non-GBM gliomas may be as effective as [^{18}F]fluoromisonidazole,[12] indicating that hypoxic imaging, including ^{62}Cu-ATSM, would be a better choice than FDG in the prediction of GBM.

However, to our knowledge, correlations between hypoxic regions depicted by PET studies and high-uptake regions in FDG or MET have not been precisely studied in GBM. In our present study, we showed that ^{62}Cu-ATSM uptake in GBM correlates significantly with FDG by volumetric assessments, but half of the uptake regions were distributed heterogeneously. Under hypoxia, glycolysis is increased by hypoxia-inducible factor-1α activation,[21] whereas in malignant tumor cells, aerobic glycolysis is driven even under nonhypoxic conditions.[2] Therefore, FDG uptake might indirectly and partially reflect hypoxic regions as well as nonhypoxic regions.[22]

In line with these observations, several clinical studies on lung and cervical cancers have directly compared ^{62}Cu-ATSM-PET with FDG-PET and suggested that intratumoral distribution and uptake values may be different, depending on the histopathologic type of the tumor.[15,23] In addition, a previous study using a lung

cancer model demonstrated that ^{64}Cu-ATSM was predominantly accumulated in hypoxic and quiescent tumor cells, a finding that differs from the FDG distribution with features of high proliferation.[24] In accordance with these findings, a hypoxic imaging study by use of [^{18}F]fluoromisonidazole revealed a positive relationship but not a precisely matched uptake to that of FDG in gliomas,[11] which seems to be similar to the results of our present study. These findings imply that the positive relationship between FDG-PET and hypoxic-PET may indicate increased glycolysis, glucose uptake, and hypoxia in GBM. In contrast, the parts of hypoxic regions not shown on FDG-PET might indicate severe ischemia and hypoxia where glucose delivery is also severely disturbed, an idea that should be explored in future investigations.

In contrast, no PET study has compared ^{62}Cu-ATSM and MET. Our present study showed that MET had larger active volumes than did ^{62}Cu-ATSM in GBM, which was fully covered within MET-active regions. There was also a significant volumetric correlation between ^{62}Cu-ATSM and MET. A volumetric correlation of MET-PET–delineated regions with hypoxic PET by [^{18}F]fluoromisonidazole has also been documented,[13] which corroborates our results. However, it is not clear why hypoxic regions delineated by ^{62}Cu-ATSM not depicted by FDG-PET still show high MET uptake. If disturbance of substrate delivery such as that of glucose is the mechanism leading to FDG-PET–negative hypoxic regions, MET delivery should also be disturbed. Multifactorial effects of tracer kinetics, such as a switch from a metabolic to a catabolic state in hypoxic tumor cells,[25] as well as a threshold setting, would cause this discrepancy in complex and heterogeneous GBMs.

From a clinical point of view, MET-PET enables more accurate delineation of glioma extension than MR imaging,[6,9] suggesting that MET is a practical radiotracer for the detection of infiltrative regions around contrast-enhanced regions on MR imaging, which can provide important clinical information for treatment. By combining ^{62}Cu-ATSM- and MET-PET imaging, delineation of hypoxic regions within MET-PET–active regions would provide additional value to delineate therapeutic targets as treatment-resistant hypoxic regions for more intensive therapy (ie, intensity-modulated radiation therapy and chemotherapy by use of convection-enhanced delivery as well as biopsy targets in GBM). However, the hypoxic mechanism is not fixed in time, and variability in spatial uptake can occur among repeated PET scans.[26] Therefore, it is crucial for PET imaging to elucidate the mechanism of changes in intratumoral radiotracer distribution as a clinical application. In addition, to confirm the differences among ^{62}Cu-ATSM, FDG, and MET in GBM, further precise metabolic evaluation within GBM is required.

Among these available imaging modalities, it is not clear which is best for distinguishing GBM from non-GBM. Contrast enhancement on MR imaging might provide a simple index; however, it is sometimes ambiguous.[27] To compare diagnostic reliability, we compared positive and negative predictive values for MR imaging, MET-PET, and ^{62}Cu-ATSM-PET and showed that for the prediction of GBM, both were higher in ^{62}Cu-ATSM than in MR imaging, indicating that ^{62}Cu-ATSM-PET is a better imaging technique for the prediction of GBM than is MR imaging. In addition, the negative predictive value was also higher for ^{62}Cu-ATSM-PET (85.7%) vs MET-PET (60.0%), though the positive values were lower. This finding would suggest that combined assessment by use of ^{62}Cu-ATSM and MET may provide a more accurate diagnosis. However, because of the small number of patients in our present study, further clinical evaluation in a larger group of patients is required to confirm these hypotheses.

Study Limitations

One of the limitations of our study was that it is unknown how BBB disruption affects ^{62}Cu-ATSM kinetics. To gain some insight, we demonstrated that the ^{62}Cu-ATSM–active volumes in GBM were significantly less than those of the contrast-enhanced volumes on MR imaging, which are dependent on BBB breakdown accompanying neovascularization in gliomas.[6] Thus, it is suggested that ^{62}Cu-ATSM uptake would be determined by other factors in addition to BBB breakdown. Indeed, it has been shown that the oxygen pressure in GBM is relatively lower than the pressure in the surrounding cortex.[28] Thus, ^{62}Cu-ATSM is likely to be a tracer that reflects part of the hypoxic region. Further clinical validation of the relationship between ^{62}Cu-ATSM uptake and tissue oxygen tension is required to determine the precision of hypoxic imaging.

In addition, our present study may have been affected by several biases, including threshold settings and MET-PET not being performed in all cases. Moreover, no published studies have compared ^{62}Cu-ATSM and [^{18}F]fluoromisonidazole for clinical use. Finally, ^{62}Cu-ATSM is rarely applicable for every institution because of limited radionuclide production. Nonetheless, multiple PET imaging by use of ^{62}Cu-ATSM, FDG, and MET may provide complementary valuable intratumoral metabolic information, all of which is important in the establishment of targeted therapeutic strategies for patients with GBM.

CONCLUSIONS

The results of our study suggest that ^{62}Cu-ATSM-PET is predictive of GBM. In addition to the information obtained by FDG-PET, MET-PET, and MR imaging, ^{62}Cu-ATSM-PET may provide intratumoral hypoxic information useful in establishing targeted therapeutic strategies for patients harboring GBM.

ACKNOWLEDGMENTS

We thank Tsuneo Saga, Masayuki Inubishi, Toshimitsu Fukumura, and Yasuhisa Fujibayashi of the Diagnostic Imaging and Molecular Probe Groups, Molecular Imaging Center, National Institute of Radiologic Sciences, Chiba, Japan; Hidehiko Okazawa of the Department of Radiology, Biomedical Imaging Research Center, Faculty of Medical Sciences, University of Fukui, Fukui, Japan; and Hirofumi Fujii, Functional Imaging Division, Research Center for Innovative Oncology, National Cancer Center Hospital East, Chiba, Japan, for their assistance.

Disclosures: Satoshi Nakanowatari—*RELATED: Grant:* Grant-in-Aid for Scientific Research from the Japan Society for the Promotion of Sciences (No. 24791515).* Nobutaka Kawahara—*RELATED: Grant:* Ministry Eduction, Culture, Sports, Science and Technology,* Comments: This grant is a public research grant offered from the Government. **Money paid to institution.*

REFERENCES

1. Louis DN, Ohgaki H, Wiestler OD, et al. **The 2007 WHO classification of tumours of the central nervous system.** *Acta Neuropathol* 2007;114:97–109
2. Plathow C, Weber WA. **Tumor cell metabolism imaging.** *J Nucl Med* 2008;49 Suppl 2:43S–63S
3. Nariai T, Tanaka Y, Wakimoto H, et al. **Usefulness of L-[methyl-11C] methionine-positron emission tomography as a biological monitoring tool in the treatment of glioma.** *J Neurosurg* 2005;103:498–507
4. Kato T, Shinoda J, Nakayama N, et al. **Metabolic assessment of gliomas using 11C-methionine, [18F] fluorodeoxyglucose, and 11C-choline positron-emission tomography.** *AJNR Am J Neuroradiol* 2008;29:1176–82
5. Delbeke D, Meyerowitz C, Lapidus RL, et al. **Optimal cutoff levels of F-18 fluorodeoxyglucose uptake in the differentiation of low-grade from high-grade brain tumors with PET.** *Radiology* 1995;195:47–52
6. Miwa K, Shinoda J, Yano H, et al. **Discrepancy between lesion distributions on methionine PET and MR images in patients with glioblastoma multiforme: insight from a PET and MR fusion image study.** *J Neurol Neurosurg Psychiatry* 2004;75:1457–62
7. Padma MV, Said S, Jacobs M, et al. **Prediction of pathology and survival by FDG PET in gliomas.** *J Neurooncol* 2003;64:227–37
8. Singhal T, Narayanan TK, Jacobs MP, et al. **11C-methionine PET for grading and prognostication in gliomas: a comparison study with 18F-FDG PET and contrast enhancement on MRI.** *J Nucl Med* 2012;53:1709–15
9. Kracht LW, Miletic H, Busch S, et al. **Delineation of brain tumor extent with [11C]L-methionine positron emission tomography: local comparison with stereotactic histopathology.** *Clin Cancer Res* 2004;10:7163–70
10. Jensen RL. **Brain tumor hypoxia: tumorigenesis, angiogenesis, imaging, pseudoprogression, and as a therapeutic target.** *J Neurooncol* 2009;92:317–35
11. Cher LM, Murone C, Lawrentschuk N, et al. **Correlation of hypoxic cell fraction and angiogenesis with glucose metabolic rate in gliomas using 18F-fluoromisonidazole, 18F-FDG PET, and immunohistochemical studies.** *J Nucl Med* 2006;47:410–18
12. Hirata K, Terasaka S, Shiga T, et al. **(18)F-Fluoromisonidazole positron emission tomography may differentiate glioblastoma multiforme from less malignant gliomas.** *Eur J Nucl Med Mol Imaging* 2012;39:760–70
13. Kawai N, Maeda Y, Kudomi N, et al. **Correlation of biological aggressiveness assessed by 11C-methionine PET and hypoxic burden assessed by 18F-fluoromisonidazole PET in newly diagnosed glioblastoma.** *Eur J Nucl Med Mol Imaging* 2011;38:441–50
14. Tateishi K, Tateishi U, Sato M, et al. **Application of ^{62}Cu-diacetyl-bis (N4-methylthiosemicarbazone) PET imaging to predict highly malignant tumor grades and hypoxia-inducible factor-1α expression in patients with glioma.** *AJNR Am J Neuroradiol* 2013;34:92–99
15. Minagawa Y, Shizukuishi K, Koike I, et al. **Assessment of tumor hypoxia by 62Cu-ATSM PET/CT as a predictor of response in head and neck cancer: a pilot study.** *Ann Nucl Med* 2011;25:339–45
16. Morooka M, Kubota K, Kadowaki H, et al. **11C-methionine PET of acute myocardial infarction.** *J Nucl Med* 2009;50:1283–87
17. Bowen SR, van der Kogel AJ, Nordsmark M, et al. **Characterization of positron emission tomography hypoxia tracer uptake and tissue oxygenation via electrochemical modeling.** *Nucl Med Biol* 2011;38:771–80
18. Fujibayashi Y, Taniuchi H, Yonekura Y, et al. **Copper-62-ATSM: a new hypoxia imaging agent with high membrane permeability and low redox potential.** *J Nucl Med* 1997;38:1155–60
19. Lewis JS, Sharp TL, Laforest R, et al. **Tumor uptake of copper-diacetyl-bis(N(4)-methylthiosemicarbazone): effect of changes in tissue oxygenation.** *J Nucl Med* 2001;42:655–61
20. Lewis JS, McCarthy DW, McCarthy TJ, et al. **Evaluation of 64Cu-ATSM in vitro and in vivo in a hypoxic tumor model.** *J Nucl Med* 1999;40:177–83
21. Ke Q, Costa M. **Hypoxia-inducible factor-1 (HIF-1).** *Mol Pharmacol* 2006;70:1469–80
22. Christian N, Deheneffe S, Bol A, et al. **Is (18)F-FDG a surrogate tracer to measure tumor hypoxia? Comparison with the hypoxic tracer (14)C-EF3 in animal tumor models.** *Radiother Oncol* 2010;97:183–88
23. Lohith TG, Kudo T, Demura Y, et al. **Pathophysiologic correlation between 62Cu-ATSM and 18F-FDG in lung cancer.** *J Nucl Med* 2009;50:1948–53
24. Oh M, Tanaka T, Kobayashi M, et al. **Radio-copper-labeled Cu-ATSM: an indicator of quiescent but clonogenic cells under mild hypoxia in a Lewis lung carcinoma model.** *Nucl Med Biol* 2009;36:419–26
25. Frezza C, Zheng L, Tennant DA, et al. **Metabolic profiling of hypoxic cells revealed a catabolic signature required for cell survival.** *PLoS One* 2011;6:e24411
26. Nehmeh SA, Lee NY, Schroder H, et al. **Reproducibility of intratumor distribution of (18)F-fluoromisonidazole in head and neck cancer.** *Int J Radiat Oncol Biol Phys* 2008;70:235–42
27. Behin A, Hoang-Xuan K, Carpentier AF, et al. **Primary brain tumours in adults.** *Lancet* 2003;361:323–31
28. Kayama T, Yoshimoto T, Fujimoto S, et al. **Intratumoral oxygen pressure in malignant brain tumor.** *J Neurosurg* 1991;74:55–59

Eur J Nucl Med Mol Imaging
DOI 10.1007/s00259-014-2714-x

ORIGINAL ARTICLE

Tumor hypoxia and microscopic diffusion capacity in brain tumors: A comparison of ^{62}Cu-Diacetyl-Bis (N4-Methylthiosemicarbazone) PET/CT and diffusion-weighted MR imaging

Ayako Hino-Shishikura · Ukihide Tateishi · Hirofumi Shibata · Tomohiro Yoneyama · Toshiaki Nishii · Ikuo Torii · Kensuke Tateishi Makoto Ohtake · Nobutaka Kawahara · Tomio Inoue

Received: 21 October 2013 / Accepted: 20 January 2014

Abstract
Objectives The aim of this study was to clarify the relationship between tumor hypoxia and microscopic diffusion capacity in primary brain tumors using ^{62}Cu-Diacetyl-Bis (N4-Methylthiosemicarbazone) (^{62}Cu-ATSM) PET/CT and diffusion-weighted MR imaging (DWI).
Methods This study was approved by the institutional human research committee and was HIPAA compliant, and informed consent was obtained from all patients. ^{62}Cu-ATSM PET/CT and DWI were performed in a total of 40 primary brain tumors of 34 patients with low grade glioma (LGG, n=13), glioblastoma (GBM, n=20), and primary central nervous system lymphoma (PCNSL, n=7). ^{62}Cu-ATSM PET/CT parameters and apparent diffusion coefficient (ADC) obtained by DWI were compared.
Results High intensity signals by ^{62}Cu-ATSM PET/CT and DWI in patients with GBM and PCNSL, and low intensity signals in LGG patients were observed. An inverse correlation was found between maximum SUV (SUV_{max}) and minimum ADC (ADC_{min}) (r=−0.583, p<0.0001), and between tumor/brain ratio (T/B_{ratio}) and ADC_{min} for all tumors (r=−0.532, p<0.0001). Both SUV_{max} and T/B_{ratio} in GBM were higher than LGG (p<0.0001 and p<0.0001), and those in PCNSL were also higher than GBM (p=0.033 and p=0.044). The ADC_{min} was lower in GBM (p=0.011) and PCNSL (p=0.01) than in LGG, while no significant difference was found between GBM and PCNSL (p=0.90).
Conclusion Tumor hypoxia assessed by ^{62}Cu-ATSM PET/CT correlated with microscopic diffusion capacity obtained by DWI in brain tumors. Both ^{62}Cu-ATSM PET/CT and DWI were considered feasible imaging methods for grading glioma. However, ^{62}Cu-ATSM PET/CT provided additional diagnostic information to differentiate between GBM and PCNSL.

Keywords ^{62}Cu-ATSM · PET/CT · Diffusion-weighted MR imaging · MRI · Glioma

Introduction

For the clinical treatment of brain tumors, currently, anatomically based imaging techniques, such as magnetic resonance imaging (MRI) and computerized tomography (CT), play major roles. Recently however, because our understanding of the molecular and cellular characteristics of tumors has advanced dramatically, the target of anti-cancer therapy has shifted to specific molecular abnormalities. Hypoxia is one of the most important molecular abnormalities in brain tumors, which seriously undermines the outcome of therapy by causing malignant progression and resistance to therapy [1–3]. Therefore, the development of new imaging procedures that are surrogates for hypoxia to predict treatment outcomes or prognosis of the disease is anticipated.

Diffusion-weighted imaging (DWI) is an MRI sequence that can visualize the random thermal motion of water molecules [4]. The utility of DWI to detect acute brain ischemia is

A. Hino-Shishikura · U. Tateishi (✉) · H. Shibata · T. Yoneyama · T. Nishii · I. Torii · T. Inoue
Department of Radiology, Graduate School of Medicine, Yokohama City University, 3-9 Fukuura, Kanazawa-ku, Yokohama 236-0004, Japan
e-mail: utateish@yokohama-cu.ac.jp

K. Tateishi · M. Ohtake · N. Kawahara
Department of Neurosurgery, Graduate School of Medicine, Yokohama City University, 3-9 Fukuura, Kanazawa-ku, Yokohama 236-0004, Japan

Published online: 10 April 2014

well known [5, 6], and several studies have reported the usefulness of apparent diffusion coefficient (ADC) to determine the World Health Organization (WHO) grade of glioma, and to predict treatment outcomes of glioma and of primary central nervous system lymphoma (PCNSL) [7–10]. To consider the usefulness of DWI in detecting brain ischemia and evaluating pathological properties of brain tumors, the capability of the application of DWI to detect hypoxic lesion is highly anticipated.

Recently, ^{62}Cu-Diacetyl-Bis (N4-Methylthiosemicarbazone) (^{62}Cu-ATSM) and ^{18}F radiolabeled fluoromisonidazole (^{18}F-FMISO), which are newly developed positron emission tomography (PET) ligands, have been reported as sensitive indicators of tumor hypoxia. The availability of these ligands has previously been reported by showing correlations with tissue pO_2 level [11–13] and with hypoxia-induced gene expression (HIF) [14]. Although several studies have revealed the availability of ^{18}F-FMISO PET for use in this setting, its clinical use is limited to specific institutions [15, 16]. ^{62}Cu-ATSM PET, which provides a more preferable imaging contrast similar to ^{18}F-FMISO, is expected to be a successful surrogate diagnostic modality for tumor hypoxia [12].

We assumed that ^{62}Cu-ATSM PET imaging and DWI show similarity and correlation. Although the utility of ^{62}Cu-ATSM in glioma has been reported in animal studies [17, 18], to date only one human clinical study that assesses the significance of ^{62}Cu-ATSM PET in glioma has been reported [19]. Furthermore, no clinical studies have been reported that discuss the correlation of ^{62}Cu-ATSM PET imaging and DWI. The aim of this study is to clarify the relationship between tumor hypoxia and microscopic diffusion capacity in primary brain tumors using ^{62}Cu-ATSM PET/CT and DWI.

Materials and methods

Patient eligibility

The Institutional Review Board of Yokohama City University Hospital approved this study (No. B1001111026), and all subjects signed a written informed consent. Thirty-four patients with primary brain tumors, who underwent both ^{62}Cu-ATSM PET/CT and DWI within 4 weeks (mean interval= 4.8 days) of each other between April 2009 and December 2012 were included in this study. The diagnosis of brain tumors was proven histologically by samples from definitive surgery. All patients underwent preoperative assessment based on a review of their medical history, physical examinations, and imaging studies, including ^{62}Cu-ATSM PET/CT and DWI. Eligible patients were those with histologically proven brain tumors, aged between 18 to 80 years with normal heart, lung, liver, and kidney function. The exclusion criteria included pregnancy, other serious medical disorders or concomitant malignancies.

MRI

MRI was performed using a 1.5 Tesla system (Magnetom Symphony; SIEMENS, Erlargen, Germany or Gyroscan Intera Master; Philips Medical Systems, Best, the Netherlands). Pulse sequences comprised of T1-weighted spin echo (SE) images (T1WI): repetition time (TR)/echo time (TE); 500–600 msec/6–10 msec, T2-weighted fast spin echo (FSE) images (T2WI): TR/effective echo time (TE_{eff}); 3120 msec/102.27 msec, as well as post-contrast T1WI with fat suppression after injection of contrast material: TR/TE; 520–645 msec/6–10 msec. Images were reconstructed in the sagittal and transaxial planes with a slice thickness of 5 mm with no intersection gaps. DWI was obtained by using spin-echo echo-planar imaging sequences (2743–3200/90–95; number of signals acquired, one; section thickness, 6 mm; gap, 1.2 mm; matrix, 99×128; field of view, 22×22 cm) with three orthogonal directional motion-probing gradients (b=1000 s/mm^2), followed by automatic generation of isotropic DWI. Images without motion-probing gradients (b=0 s/mm^2) were simultaneously obtained as well. ADCs were calculated using software incorporated in the MR imaging unit.

Radiopharmaceuticals

The ^{62}Cu-glycine (no-carrier-added ^{62}Cu) solution was obtained from a ^{62}Zn/^{62}Cu generator system supplied by the National Institute of Radiological Sciences (NIRS). ^{62}Cu-ATSM was prepared using a simple mixture of 5 mL of ^{62}Cu solution and 0.2 mL of ATSM solution (0.5 mM in dimethyl sulfoxide) in a sterilized vial. Unlabeled Cu-ATSM was used to determine the retention time. Quality control of ^{62}Cu-ATSM included high performance liquid chromatography (HPLC) prior to the first patient injection.

PET/CT

A phantom PET/CT study was performed to clarify the necessary and sufficient conditions for data acquisition and to ensure quality control before the clinical study. Studies were performed with a whole-body PET/CT scanner (Aquiduo PCA-7000B, Toshiba) with a CT component having a 16-row detector. We performed a phantom study to obtain an estimation of the optimum time. The radioactivity concentration of the background was set similarly to that in clinical conditions. Acquired data, including the normalization data, cross-calibration data, blank scan data and transmission data, were assessed for visual inspection, phantom noise equivalent count ($NEC_{phantom}$), % contrast ($Q_{H,\ 10mm}$) and % background variability (N_{10mm}). After a review of the data analyses, the

optimum conditions for the PET/CT were also determined: data acquisition, 180 s for one bed; FOV, 500 mm; iteration, 4; subset, 14; matrix size,128×128; filter, Gaussian 8 mm in FWHM; reconstruction, OSEM. Patients received an intravenous injection of 740 MBq of ^{62}Cu-ATSM. The patients were then placed in a supine, arm-down position. Dynamic scans for 30 min were performed after injection, and the data acquired for 20 to 30 min was reconstructed for PET/CT images to minimize the effect of cerebral blood flow [19]. Time decay correction was performed automatically. The axial field of view of the scanner was 18 cm. For the PET/CT, low-dose CT data was first acquired at 120-kVp using an auto exposure control system, 0.5 s per CT rotation, with a beam pitch of 1.0 and 2-mm×16-row mode. Data acquisition was performed for the entire brain for each patient.

Image interpretation

MR images were evaluated by two board-certified radiologists (with 16 and 12 years of experience, respectively). MR findings from the primary tumor were assessed using a Synapse workstation (FUJIFILM Medical Co., Ltd., Tokyo, Japan). The patterns of signal intensity on each sequence, and post-contrast T1WI were evaluated. To analyze ADC values, regions of interest (ROIs) were manually drawn on the outline of tumors on all continuous sections of the post-contrast T1WI, and subsequently copied to ADC maps. The cystic, necrotic or hemorrhagic components within tumors were carefully avoided by visual inspection. The minimum ADC value (ADC_{min}) within ROIs was measured according to previous studies [8, 10].

The PET and CT images in all standard planes were reviewed on workstations (FUJIFILM Medical Co., Ltd., Tokyo, Japan, PETSTAT™ and AdIn Research, Inc., Tokyo, Japan). Images were analyzed visually and quantitatively by two nuclear medicine physicians (with 18 and 10 years of experience, respectively), who, after reaching a consensus, recorded their findings. For the visual analysis, abnormal ^{62}Cu-ATSM uptake was defined as activity substantially greater than contralateral normal brain tissue on the attenuation-corrected images. Only the lesion that exhibited the most significant uptake was selected. ROIs were outlined within areas of increased ^{62}Cu-ATSM uptake and measured on each slice. PET images were overlaid directly on diffusion-weighted images and ADC maps. If lesions were extensively heterogeneous, the ROI was set to cover all of the components of the lesion. Qualitative evaluation of the standardized uptake value (SUV) was performed to evaluate tumor hypoxia. The SUV was calculated according to the following equation: SUV=maximal count×calibration factor (kBq/ml)/injected activity (MBq)/body weight (kg). To evaluate the concentration of ^{62}Cu-ATSM, the maximum SUV (SUV_{max}) and the Tumor/Brain ratio (T/B_{ratio}) were measured. The SUV_{max} was measured as the maximum value of SUV within the ROI. The T/B_{ratio} was calculated by dividing mean SUV of the tumor with the mean SUV value of the normal contralateral lobe.

Patterns of ^{62}Cu-ATSM uptake, signal intensity of DWI and enhancement on post-contrast T1WI were visually evaluated and classified into five patterns, according to the location of accumulation in PET/CT and high signal intensity in DWI: overall type (homogenous or heterogeneous accumulation in PET/CT or high signal intensity in DWI in whole tumor); peripheral focal type (accumulation in PET/CT or high signal intensity in DWI in part of the tumor margin); marginal type (accumulation in PET/CT or high signal intensity in DWI along the entire of the tumor margin), central type (accumulation or high signal intensity in the center of the tumor), negative type (no accumulation in the tumor).

Reference standard

Samples from the tumor were obtained at the time of definitive surgery. Merged ^{62}Cu-ATSM PET/CT images were exported to a neuronavigation system (StealthStation, Medtronic Sofamor Danek) for precise tissue sampling of the lesion representing strong accumulation of ^{62}Cu-ATSM. Histological slices 4 μm in thickness were cut, stained with hematoxylin-eosin, and examined with light microscopy. Tumor specimens were immunostained with Ki-67 antibody (clone MIB-1; DakoCytomation; diluted 1:100 and autoclaved) to determine pathologic diagnosis and the Ki-67 (MIB-1) labeling index was estimated as subsidiary measures by calculating the percentage of Ki-67 positive cell nuclei among 1,000 tumor cells in the region of the tumor in which the greatest density of MIB-1 staining was observed under a light microscope. The mean interval between the PET study and either surgical resection or biopsy was 2.3 days (range, 1–8 days).

Statistical analysis

All PET and ADC data were expressed as mean ± standard deviation (SD). Correlations between ADC_{min} and SUV_{max}, ADC_{min} and T/B_{ratio} were measured by calculating the Pearson product–moment correlation coefficients. A Student's *t* test was applied to assess the difference of SUV_{max}, T/B_{ratio} and the ADC_{min} between tumor subtypes.

Agreement between reviewers within a patient group was measured by a Cohen's kappa (k) and McNemar's test. Kappa values were interpreted as suggested by Altman: < 0.20 poor agreement; 0.21–0.40 fair agreement; 0.41–0.60 moderate agreement; 0.61–0.80 good agreement; and 0.81–1.00 excellent agreement.

All p values presented were calculated via a two-sided test and were adjusted for multiple testing using Bonferroni's correction. For all analyses, a $P<0.05$ was considered to denote a significant difference. Statistical analyses were performed with PETSTAT ™ (AdIn Research, Inc., Tokyo, Japan) and the PASW Statistics 19 software program (IBM, Tokyo, Japan).

Results

The analyses were based on data obtained from 40 tumors in 34 patients (18 men and 16 women) (Table 1). Of these, 17 patients (50.0 %) were newly diagnosed, and the remaining 17 patients (50.0 %) were diagnosed as having tumor recurrence with histological confirmation. The mean age of patients was

Table 1 Patient demographics

Case No.	Age	Sex	Chief complaint at the time of fist admission	Histological diagnosis	Tumor type	Tumor number	Tumor location	Tumor size (cm)
1	38	M	Syncope	LGG	new	1	lt. frontal	5.0
2	73	F	Dementia	LGG	new	1	transparent septum	5.0
3	59	M	Seizure	LGG	rec	1	rt. occipital	3.6
4	23	F	Consciousness disorder	LGG	new	1	rt. frontal	2.0
5	69	F	Seizure	LGG	rec	2	lt. frontal, lt. frontal	3.3, 3.5
6	70	F	Headache, nausea	LGG	rec	2	transparent septum, lt. frontal	3.5, 2.2
7	19	M	Fever, seizure	LGG	new	1	rt. temporal	5.0
8	43	M	Memory disturbance	LGG	new	1	lt. frontal	2.2
9	47	M	Headache, syncope	LGG	new	1	rt. insula	2.5
10	45	M	Numbness of right hand	LGG	new	1	lt. parietal	2.3
11	66	F	Diplopia, disorientation	LGG	rec	1	lt. thalamus	3.5
12	59	F	Memory disturbance, lt. hemiplegia	GBM	new	1	rt. temporal	5.0
13	63	M	lt. hemiplegia	GBM	new	1	rt. thalamus	3.4
14	77	M	Dysphasia	GBM	new	1	lt. temporal	2.5
15	61	F	lt. homonymous hemianopia	GBM	new	1	rt. temporal	4.5
16	61	F	Headache	GBM	new	1	rt. temporal	2.6
17	75	F	Memory disturbance	GBM	rec	1	lt. callosum	2.0
18	75	F	Difficulty in walking, consciousness disorder	GBM	rec	1	lt. callosum	3.0
19	59	M	lt. hemiplegia	GBM	rec	1	rt. frontal	2.6
20	59	M	lt. hemiplegia	GBM	rec	1	rt. frontal	2.5
21	59	F	lt. conjugate deviation, rt. hemiplegia	GBM	rec	1	lt. parietal	1.8
22	59	F	Consciousness disorder	GBM	rec	3	rt. frontal, lt. parietal, rt. frontal	2.0, 3.0, 2.5
23	28	F	Headache, nausea	GBM	new	1	rt. frontal	2.5
24	40	M	Fever, headache	GBM	rec	1	rt. callosum	2.2
25	40	M	General malaise	GBM	rec	1	rt. occipital	2.0
26	40	M	Sensory abnormality, lt. paresis	GBM	rec	1	rt. occipital	2.0
27	60	F	rt. homonymous hemianopia	GBM	new	1	lt. thalamus	4.0
28	59	M	Headache	GBM	new	1	rt. temporal	3.7
29	65	M	Dysphasia, lt. paralysis	GBM	rec	1	rt. occipital	2.2
30	68	F	Dysstasia, consciousness disorder	PCNSL	rec	2	rt. temporal, lt. parietal	1.7, 2.6
31	79	F	Disorientation, rt. hemiplegia, gait disturbance	PCNSL	new	1	callosum	4.4
32	41	M	Upper extremity weakness, facial spasm	PCNSL	rec	1	rt. parietal	3.8
33	45	M	Consciousness disorder	PCNSL	new	1	lt. parietal	4.0
34	65	M	Dysphasia, lt. paralysis	PCNSL	rec	2	rt. frontal, lt. occipital	2.5, 2.0

LGG low grade glioma; GBM glioblastoma multiforme; PCNSL primary central nervous system lymphoma; New newly diagnosed; Rec recurrent; rt. right; lt. left; frontal frontal lobe; parietal parietal lobe; occipital occipital lobe; temporal temporal lobe

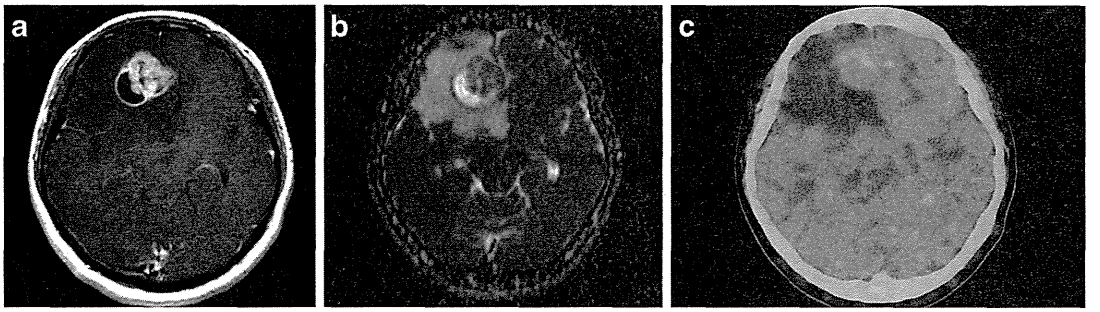

Fig. 1 Images from a 28-year-old man with GBM. **a** Axial post-contrast T1WI shows a solid and cystic mass in the right frontal lobe. Strong heterogeneous enhancement is shown within the solid component and surrounding cystic area. **b** ADC map of the tumor shows reduced ADC value in part of the tumor margin ($ADC_{min}=840\times10^{-6}$ mm^2/s). **c** ^{62}Cu-ATSM PET/CT also shows mild accumulation in part of the tumor margin ($SUV_{max}=1.20$, $T/B_{ratio}=1.70$)

56.0±14.8 years. Finally, a total of 40 tumors were analyzed and up to three tumors were included from each patient. Tumor subtypes were as follows; 11 patients had 13 low grade gliomas (LGG); 18 had 20 glioblastomas (GBM); and five had seven primary central nervous system lymphomas (PCNSL). The mean tumor diameter was 3.0±1.0 cm.

By visual analyses, Cohen's kappa (k) values of ^{62}Cu-ATSM PET/CT, DWI, and post-contrast T1WI were 0.76, 0.68, and 0.71, respectively. The representative ^{62}Cu-ATSM PET/CT, DWI and post-contrast T1WI images are shown in Figs. 1 and 2. For LGG, a relatively low accumulation was observed via ^{62}Cu-ATSM PET/CT, and DWI images also showed low signal intensity as compared with normal brain tissue. For GBM and PCNSL, tumors demonstrated high accumulation on ^{62}Cu-ATSM PET/CT and hyper signal intensity on DWI.

For all tumors, the mean SUV_{max} of ^{62}Cu-ATSM PET/CT was 1.52±0.70, and the mean T/B_{ratio} was 2.53±1.63. The mean SUV_{max} was 0.90±0.25 in LGG, 1.68±0.68 in GBM, and 2.17±0.39 in PCNSL. The mean SUV_{max} in patients with GBM was higher than in those with LGG ($p<0.0001$, Fig. 3). The mean SUV_{max} in patients with PCNSL was higher than in those with LGG ($p<0.0001$, Fig. 3) and those with GBM ($p=0.033$, Fig. 3). The mean T/B_{ratio} was 1.23±0.34 in LGG, 2.84±1.72 in GBM, and 4.03±1.04 in PCNSL. Similar trends in mean SUV_{max} for different histologic types were also found, similar to T/B_{ratio}. The mean T/B_{ratio} in patients with GBM was significantly higher than in those with LGG ($p<0.0001$). The mean T/B_{ratio} in PCNSL was higher than in LGG ($p<0.0001$). The mean T/B_{ratio} was also higher in PCNSL than in GBM ($p=0.044$, Fig. 3).

For all tumor types, the mean ADC_{min} was 80.8±25.6. The mean ADC_{min} was 98.4±36.4 in LGG, 68.2±12.6 in GBM, and 67.7±7.0 in PCNSL. Significant differences were found in the mean ADC_{min} between GBM and LGG ($p=0.011$, Fig. 3) and between PCNSL and LGG ($p=0.01$, Fig. 3). ADC_{min} was lowest in PCNSL and highest in LGG, but there was no significant difference in ADC_{min} between GBM and PCNSL ($p=0.90$, Fig. 3). For all tumors, inverse correlations were found between both SUV_{max} and ADC_{min} ($r=-0.583$, $p<0.0001$), as well as T/B_{ratio} and ADC_{min} ($r=-0.532$, $p<0.0001$, Fig. 4).

The patterns of uptake and signal intensity on ^{62}Cu-ATSM PET/CT, DWI and post-contrast T1WI are summarized in Table 2. For the distribution of intensity for LGG, the peripheral focal type was most frequent and the negative type was followed on ^{62}Cu-ATSM PET/CT, while the patterns of high signal intensity in DWI and post-contrast T1WI were diverse and no consistency was found. For the uptake and signal intensity in these imaging modalities for GBM, the peripheral

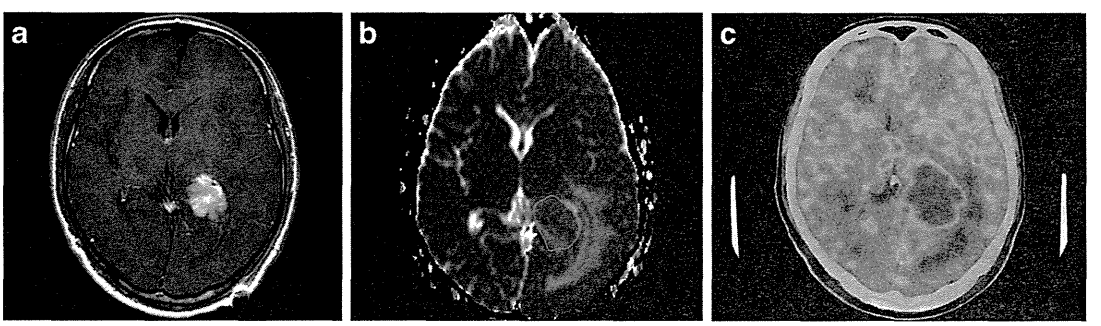

Fig. 2 Images from a 45-year-old man with PCNSL. **a** Axial post-contrast T1WI shows a solid mass in the left parietal lobe, which shows very strong contrast enhancement in the solid component. **b** ADC reduction is shown overall in the tumor on the ADC map ($ADC_{min}=693\times10^{-6}$ mm^2/s). **c** ^{62}Cu-ATSM PET/CT also shows a strong and heterogeneous overall uptake in the tumor ($SUV_{max}=2.50$, $T/B_{ratio}=5.20$)

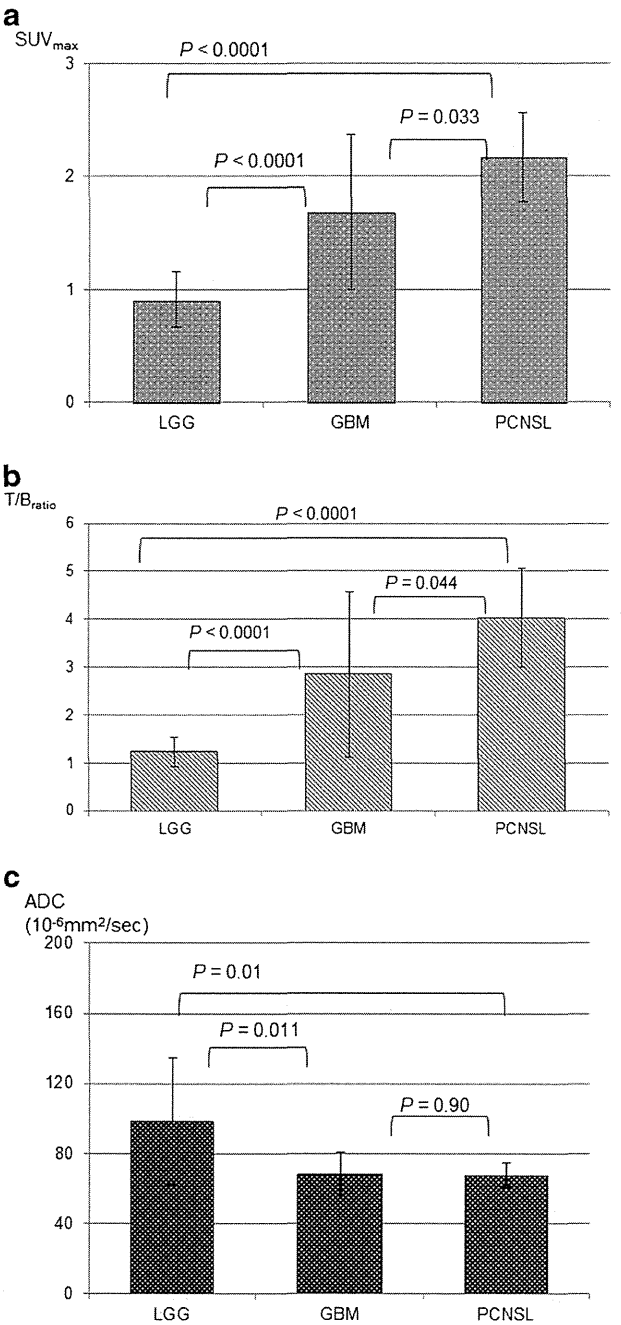

Fig. 3 **a** A comparison of SUV_{max} by ^{62}Cu-ATSM PET/CT between GBM, LGG and PCNSL. SUV_{max} was significantly higher in GBM than in LGG ($p<0.0001$). SUV_{max} was also significantly higher in PCNSL than in GBM ($p=0.033$). **b** A comparison of T/B_{ratio} by ^{62}Cu-ATSM PET/CT between GBM, LGG and PCNSL. T/B_{ratio} was significantly higher in GBM than in LGG ($p<0.0001$). T/B_{ratio} was also significantly higher in PCNSL than in GBM ($p=0.044$). **c** A comparison of ADC_{min} by DWI between GBM, LGG and PCNSL. ADC_{min} was significantly lower in GBM than in LGG ($p=0.011$). No significant difference was found between PCNSL and GBM ($p=0.90$)

focal type was most frequent, and the overall type was followed both on ^{62}Cu-ATSM PET/CT and DWI. When comparing

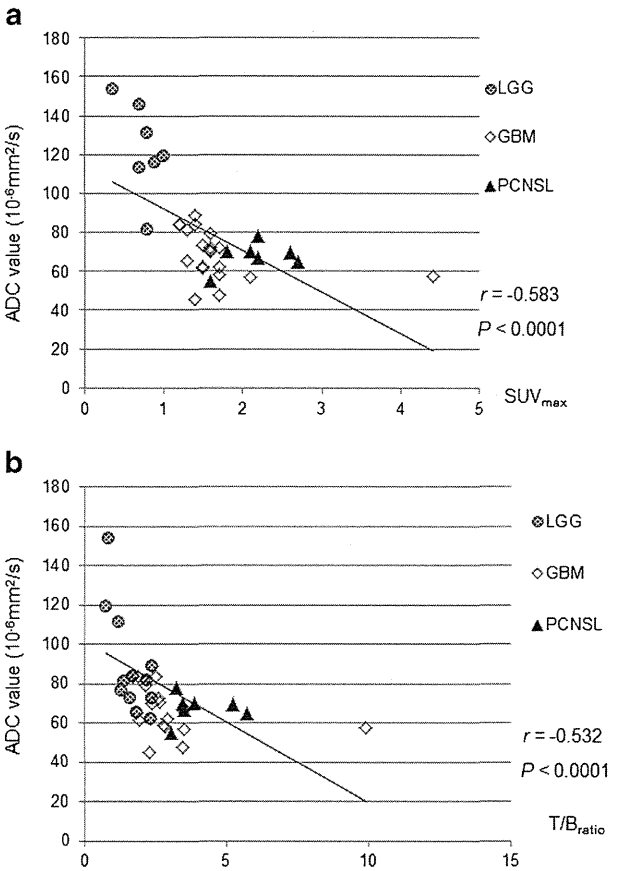

Fig. 4 **a** The correlation of the SUV_{max} by ^{62}Cu-ATSM PET/CT and ADC_{min} by DWI. Moderate inverse correlation was exhibited for all tumors ($r=-0.583$, $p<0.0001$). **b** The correlation of T/B_{ratio} by ^{62}Cu-ATSM PET/CT and ADC_{min} by DWI. Moderate inverse correlation was also exhibited for all tumors ($r=-0.532$, $p<0.0001$)

post-contrast T1WI of GBM, the peripheral focal type was slightly more frequent, and ring type and overall type were followed. For PCNSL, the patterns of uptake and signal intensity were similar in all three imaging modalities, and the overall type was most frequent.

Discussion

Our data show that tumor hypoxia according to metabolism by ^{62}Cu-ATSM PET/CT correlates with microscopic diffusion capacity by DWI in primary brain tumors. The results of comparative analyses in our study identified that accumulation on ^{62}Cu-ATSM PET/CT was high in GBM and PCNSL, and low in LGG. On the other hand, high signal intensity, as measured by DWI, was observed in GBM and PCNSL, whereas low signal intensity was observed in LGG. When focusing on the pronounced intensity on ^{62}Cu-ATSM PET/CT imaging and DWI, these two imaging modalities reflect correlations between tumor hypoxia, microscopic diffusion capacity, and malignancy or aggressiveness in primary brain tumors.

Table 2 The patterns of distribution of ^{62}Cu-ATSM PET/CT uptake, enhanced signal intensity of diffusion weighted image and contrast enhanced T1-weighted image

Diagnosis	^{62}Cu-ATSM PET/CT	Number	DWI	Number	Post contrast T1WI	Number
LGG (n=13)	Negative	5 (38.5)	Negative	4 (30.8)	Negative	3 (23.1)
	Marginal	0	Marginal	4 (30.8)	Marginal	3 (23.1)
	Peripheral focal	6 (46.2)	Peripheral focal	2 (15.4)	Peripheral focal	3 (23.1)
	Central	2 (15.4)	Central	1 (7.7)	Central	1 (7.7)
	Overall	0	Overall	2 (15.4)	Overall	3 (23.1)
GBM (n=20)	Negative	0	Negative	0	Negative	0
	Marginal	0	Marginal	0	Marginal	6 (30.0)
	Peripheral focal	13 (65.0)	Peripheral focal	14 (70.0)	Peripheral focal	8 (40.0)
	Central	1 (5.0)	Central	2 (10.0)	Central	0
	Overall	6 (30.0)	Overall	4 (20.0)	Overall	6 (30.0)
PCNSL (n=7)	Negative	0	Negative	0	Negative	0
	Marginal	0	Marginal	2 (28.6)	Marginal	0
	Peripheral focal	0	Peripheral focal	1 (14.3)	Peripheral focal	0
	Central	0	Central	0	Central	0
	Overall	7 (100.0)	Overall	4 (57.1)	Overall	7 (100.0)

The numbers in the parentheses are percentages. *LGG* low grade glioma; *GBM* glioblastoma multiforme; *PCNSL* primary central nervous system lymphoma; *DWI* diffusion-weighted image; *T1WI* T1-weighted image

Both differences and similarities were pointed out when comparing the types of distribution of high intensity in ^{62}Cu-ATSM PET/CT, DWI and post-contrast T1WI. When comparing the images of GBM, the peripheral focal type was dominant both in DWI and ^{62}Cu-ATSM PET/CT, while all types were shown in almost similar frequency in post-contrast T1WI. This discrepancy may be a result of a large proportion of irreversible necrosis in the GBM tissue [20, 21]. The low accumulation of ^{62}Cu-ATSM in irreversible necrosis has previously been reported using myocardial infarction animal experimental models [22], and it is also well known that brain stroke has a high intensity on DWI only in the acute stage [23]. Furthermore, some studies have already revealed that Cu-ATSM uptake of tumor tissue is heterogeneous and complex, and our data corresponds well those reports in this regard [24, 25]. It is assumed that the hypoxic but not irreversibly necrotic areas may be located sparsely on the margin of the GBM tissue, while irreversible necrosis may be located in the center of the tumor. For PCNSL, the overall type was dominant in all imaging modalities. This similarity may also be a result of high cellularity and the angiocentric growth pattern of PCNSL [26].

When comparing the SUV_{max} and T/B_{ratio} of ^{62}Cu-ATSM PET/CT with ADC_{min}, an inverse correlation was shown (Fig 3). These results may confirm the feasibility of quantitative assessment of similar biological characteristics in brain tumors, though applying two different imaging techniques. The possible explanation for this negative correlation is the diversity of cellular attenuation of tumor tissues, which have different malignant potentials. In rapidly proliferating and highly cellular tumors, metabolic demand outweighs the vascular supply of oxygen and an alteration of the energy producing process from the TCA cycle to glycolysis occurs, where nicotinamide adenine dinucleotide (NADH) is produced [27]. The accelerated NADH rapidly reduces Cu(II)-ATSM to Cu(I)-ATSM, which is then entrapped in the cells and shows significantly high contrast images on ^{62}Cu-ATSM PET/CT. On the other hand, the correlation of ADC reduction with high cellularity in brain tumors has been previously reported [9, 10, 28]. Therefore, the tumor hypoxia represented by ^{62}Cu-ATSM PET/CT possibly corresponds to restricted water diffusion represented by ADC reduction.

When evaluating the differences in SUV_{max}, T/B_{ratio} and ADC_{min} between tumor subtypes, significant differences were shown between LGG and GBM, both in ^{62}Cu-ATSM accumulation and ADC value. This result indicates the feasibility of the application of ^{62}Cu-ATSM PET for WHO tumor grading. Our data also demonstrate that the SUV_{max} and T/B_{ratio} were significantly higher in PCNSL than in GBM, while there was no significant difference in ADC_{min}. Similar results have been reported using FDG-PET and similar MRI findings reported using ADC measurements of PCNSL and GBM [29]. We assume that the possible reason for this discrepancy is the difference of the proportion of irreversible necrosis within tumor tissues between GBM and PCNSL. As mentioned above, GBM tissue characteristically contains bulk necrosis, while PCNSL shows high cellularity [3, 20, 21, 26]. Presumably, the accumulation of PET ligands such as FDG and ^{62}Cu-ATSM is reduced more sensitively on the boundary between the areas with proliferating cells and irreversible necrosis, while the restriction of water diffusion is sometimes similar.

The recent introduction of integrated whole-body PET/MRI systems enables us to perform more precise metabolic–anatomic correlation in clinical practice [30, 31]. PET/MRI would be highly accurate in detecting hypoxic lesions with ^{62}Cu-ATSM. By adding direct information from microscopic diffusion capacity to PET, diagnostic accuracy in differentiating between hypoxic and non-hypoxic lesions can be improved. However, the image quality of PET/MRI depends on many factors and may be guaranteed by optimization of imaging conditions and standardization of quality controls.

This study includes several potential limitations. It must be emphasized that our study focused on a limited number of patients with brain tumors who underwent both ^{62}Cu-ATSM PET and DWI, and the data cannot simply be extrapolated to all patients. Another potential bias may arise because the diverse treatment regimens for disease between patients, primal and recurrent tumors were not identified in this study. However, these are common limitations because of the clinical need for multiple treatment regimens. More importantly, the usefulness of ^{62}Cu-ATSM PET/CT and DWI in reducing the number of ineffective chemotherapies in patients without response must be revealed by further validation in a multicenter trial to clarify the cost-effectiveness.

Conclusion

^{62}Cu-ATSM PET/CT and DWI were performed on patients with brain tumors. Images from ^{62}Cu-ATSM PET/CT and DWI show similarity, and ^{62}Cu-ATSM uptake correlated significantly with ADC reduction. Both ^{62}Cu-ATSM PET/CT and DWI can be considered good diagnostic tests for grading gliomas. For the differential diagnosis of GBM and PCNSL, SUV measurement of ^{62}Cu-ATSM PET/CT may provide additional information. The feasibility of the application of ^{62}Cu-ATSM PET/CT to predict tumor malignancy in primary brain tumors is suggested.

Acknowledgments The authors declare that they have no conflicts of interest. We thank Tsuneo Saga, Masayuki Inubishi, Toshimitsu Fukumura, and Yasuhisa Fujibayashi of the Diagnostic Imaging and Molecular Probe Groups, Molecular Imaging Center, National Institute of Radiologic Sciences, Chiba, Japan; Hidehiko Okazawa of the Department of Radiology, Biomedical Imaging Research Center, Faculty of Medical Sciences, University of Fukui, Fukui, Japan; and Hirofumi Fujii, Functional Imaging Division, Research Center for Innovative Oncology, National Cancer Center Hospital East, Chiba, Japan, for their assistance. We also thank our nuclear medicine technologists for acquiring PET/CT scans. This work was also supported (in part) by a Grant-in-Aid for Cancer Research (21-5-2) from the Ministry of Health, Labour and Welfare.

References

1. Graeber TG, Osmanian C, Jacks T, et al. Hypoxia-mediated selection of cells with diminished apoptotic potential in solid tumours. Nature. 1996;379:88–91.
2. Shweiki D, Itin A, Soffer D, et al. Vascular endothelial growth factor induced by hypoxia may mediate hypoxia-initiated angiogenesis. Nature. 1992;359:843–5.
3. Jensen RL. Brain tumor hypoxia: tumorigenesis, angiogenesis, imaging, pseudoprogression, and as a therapeutic target. J Neurooncol. 2009;92:317–35.
4. Le Bihan D, Breton E, Lallemand D, et al. MR imaging of intravoxel incoherent motions: application to diffusion and perfusion in neurologic disorders. Radiology. 1986;161:401–7.
5. Warach S, Chien D, Li W, Ronthal M, et al. Fast magnetic resonance diffusion-weighted imaging of acute human stroke. Neurology. 1992;42:1717–23.
6. Pierpaoli C, Righini A, Linfante I, et al. Histopathologic correlates of abnormal water diffusion in cerebral ischemia: diffusion-weighted MR imaging and light and electron microscopic study. Radiology. 1993;189:439–48.
7. Khayal IS, Vandenberg SR, Smith KJ, et al. MRI apparent diffusion coefficient reflects histopathologic subtype, axonal disruption, and tumor fraction in diffuse-type grade II gliomas. Neuro Oncol. 2011;13:1192–201.
8. Murakami R, Hirai T, Sugahara T, et al. Grading astrocytic tumors by using apparent diffusion coefficient parameters: superiority of a one- versus two-parameter pilot method. Radiology. 2009;251:838–45.
9. Barajas Jr RF, Rubenstein JL, Chang JS, et al. Diffusion-weighted MR imaging derived apparent diffusion coefficient is predictive of clinical outcome in primary central nervous system lymphoma. Am J Neuroradiol. 2010;31:60–6.
10. Higano S, Yun X, Kumabe T, et al. Malignant astrocytic tumors: clinical importance of apparent diffusion coefficient in prediction of grade and prognosis. Radiology. 2006;241:839–46.
11. Hoigebazar L, Jeong JM. Hypoxia imaging agents labeled with positron emitters. Recent results. Cancer Res. 2012;194:285–99.
12. Fujibayashi Y, Taniuchi H, Yonekura Y, et al. Copper-62-ATSM: a new hypoxia imaging agent with high membrane permeability and low redox potential. J Nucl Med. 1997;38:1155–60.
13. Imam SK. Review of positron emission tomography tracers for imaging of tumor hypoxia. Cancer Biother Radiopharm. 2010;25:365–74.
14. Wen B, Burgman P, Zanzonico P, et al. A preclinical model for noninvasive imaging of hypoxia-induced gene expression; comparison with an exogenous marker of tumor hypoxia. Eur J Nucl Med Mol Imaging. 2004;31:1530–8.
15. Nunn A, Linder K, Strauss HW. Nitroimidazoles and imaging hypoxia. Eur J Nucl Med. 1995;22:265–80.
16. Martin GV, Caldwell JH, Graham MM, et al. Noninvasive detection of hypoxic myocardium using fluorine-18-fluoromisonidazole and positron emission tomography. J Nucl Med. 1992;33:2202–8.
17. Sheehan JP, Popp B, Monteith S, et al. Trans sodium crocetinate: functional neuroimaging studies in a hypoxic brain tumor. J Neurosurg. 2011;115:749–53.
18. Lewis JS, Sharp TL, Laforest R, et al. Tumor uptake of copper-diacetyl-bis(N(4)-methylthiosemicarbazone): effect of changes in tissue oxygenation. J Nucl Med. 2001;42:655–61.
19. Tateishi K, Tateishi U, Sato M, et al. Application of 62Cu-Diacetyl-Bis (N4-Methylthiosemicarbazone) PET imaging to predict highly malignant tumor grades and hypoxia-inducible factor-1alpha expression in patients with glioma. Am J Neuroradiol. 2012;34:92–9.
20. Brat DJ, Van Meir EG. Vaso-occlusive and prothrombotic mechanisms associated with tumor hypoxia, necrosis, and accelerated growth in glioblastoma. Lab Invest. 2004;84:397–405.

21. Louis DN, Ohgaki H, Wiestler OD, et al. The 2007 WHO classification of tumours of the central nervous system. Acta Neuropathol. 2007;114:97–109.
22. Fujibayashi Y, Cutler CS, Anderson CJ, et al. Comparative studies of Cu-64-ATSM and C-11-acetate in an acute myocardial infarction model: ex vivo imaging of hypoxia in rats. Nucl Med Biol. 1999;26:117–21.
23. Read SJ, Jackson GD, Abbott DF, et al. Experience with diffusion-weighted imaging in an acute stroke unit. Cerebrovasc Dis. 1998;8:135–43.
24. Lewis JS, McCarthy DW, Welch MJ, et al. Evaluation of 64Cu-ATSM in vitro and in vivo in a tumor model. J Nucl Med. 1999;40:177–83.
25. Yuan H, Schroeder T, Bowsher JE, Dewhirst MW, et al. Intertumoral differences in hypoxia selectivity of the PET imaging agent 64Cu(II)-diacetyl-bis(N4-methylthiosemicarbazone). J Nucl Med. 2006;47:989–98.
26. Schlegel U, Schmidt-Wolf IG, Deckert M. Primary CNS lymphoma: clinical presentation, pathological classification, molecular pathogenesis and treatment. J Neurol Sci. 2000;181:1–12.
27. Barlow CH, Harken AH, Chance B. Evaluation of cardiac ischemia by NADH fluroescence photography. Ann Surg. 1977;186:737–40.
28. Guo AC, Cummings TJ, Dash RC, et al. Lymphomas and high-grade astrocytomas: comparison of water diffusibility and histologic characteristics. Radiology. 2002;224:177–83.
29. Matsushima N, Maeda M, Umino M, et al. Relation between FDG uptake and apparent diffusion coefficients in glioma and malignant lymphoma. Ann Nucl Med. 2012;26:262–71.
30. Buchbender C, Heusner TA, Lauenstein C, et al. Oncologic PET/MRI, Part 1: tumor of the brain, head and neck, chest, abdomen, and pelvis. J Nucl Med. 2012;53:928–38.
31. Buchbender C, Heusner TA, Lauenstein C, et al. Oncologic PET/MRI, Part 2: bone tumors, soft-tissue tumors, melanoma, and lymphoma. J Nucl Med. 2012;53:1244–52.